Optimization of Coal Particle Flow Patterns in Low NO_x Burners

Technical Progress Report

Due April 30, 2000

Prepared by

Jost O.L. Wendt and Gregory E. Ogden
Dept. of Chemical & Environmental Engineering
University of Arizona
Tucson, AZ 85721

Jennifer Sinclair and Stephanus Budilarto
School of Chemical Engineering
Purdue University
West Lafayette, IN 47907

Submitted to

DOCUMENT CONTROL CENTER,
U.S. Department of Energy
University Coal Research Program
Pittsburgh Energy Research Center
P.O. Box 10940, MS 921-0940
Pittsburgh, PA 15236-0940.

Under Contract DE-FG26-97FT97269

August 20, 2001

INTRODUCTION

The proposed research is directed at evaluating the effect of flame aerodynamics on NO_x emissions from coal fired burners in a systematic manner. This fundamental research includes both experimental and modeling efforts being performed at the University of Arizona in collaboration with Purdue University. The objective of this effort is to develop rational design tools for optimizing low NO_x burners to the kinetic emissions limit (below 0.2 lb./MMBTU). Experimental studies include both cold and hot flow evaluations of the following parameters: flame holder geometry, secondary air swirl, primary and secondary inlet air velocity, coal concentration in the primary air and coal particle size distribution. Hot flow experiments will also evaluate the effect of wall temperature on burner performance.

Cold flow studies will be conducted with surrogate particles as well as pulverized coal. The cold flow furnace will be similar in size and geometry to the hot-flow furnace but will be designed to use a laser Doppler velocimeter/phase Doppler particle size analyzer. The results of these studies will be used to predict particle trajectories in the hot-flow furnace as well as to estimate the effect of flame holder geometry on furnace flow field. The hot-flow experiments will be conducted in a novel near-flame down-flow pulverized coal furnace. The furnace will be equipped with externally heated walls. Both reactors will be sized to minimize wall effects on particle flow fields.

The cold-flow results will be compared with Fluent computation fluid dynamics model predictions and correlated with the hot-flow results with the overall goal of providing insight for novel low NO_x burner geometry's.

CURRENT PROGRESS

Experimental shakedown tests continue utilizing natural gas and heated combustion air at the University of Arizona. The bulk of the project efforts during this period were at Purdue University as noted below.

Computational Results and Discussions

a) Single-Phase Coaxial Jet

A computational study using the Fluent 4.5 CFD package was performed to evaluate the predictive capability of the standard k-ε turbulent model for the coaxial jet flow behavior. It is important to have an accurate solution for the single-phase flow since it will be used to calculate the particle trajectory. The Fluent 4.5 CFD package discretizes the governing equation in space using a finite volume formulation. The standard k-ε model relates the Reynolds stress using the Boussinesq eddy viscosity assumption. The Boussinesq eddy-viscosity model defines the Reynolds stress to be proportional to the mean velocity gradient. The model also lacks a way to distribute the turbulent kinetic energy among the different components; hence, it does not predict anisotropic turbulence. The ability of the model to predict anisotropic jet behavior is however, important since the radial gas fluctuating velocity, v_g' may be responsible for the radial motion of particles.

The boundary conditions at the inlet were matched with the experimental results. A no-slip boundary condition was applied at the solid wall and the wall function was used to approximate the near wall solution. A zero-gradient was applied for the outlet boundary condition. The calculation used 40x500 grid points in the radial and axial direction, respectively. This grid resolution shown in Figure 1 has yielded a grid-independent solution. The radial grid is clustered along all solid walls and stretched between the solid walls for the whole length.

Results and Discussion

Figures 2 and 3 shows the axial evolution of the axial mean gas velocity and the gas turbulence kinetic energy along jet centerline, respectively. It shows that the standard k-ε model overpredicts the gas turbulent kinetic energy and causes the underprediction of the axial mean gas velocity for the case with velocity ratio of 0. For the velocity ratio of 1.8, the standard k-ε underpredicts the gas turbulent kinetic energy along the centerline between $0 < x/d_i < 10$. Consequently, the axial mean gas is not accelerated as fast as that observed in the experiment. For the case with velocity ratio of 1, the standard k-ε model underpredict the axial evolution of gas turbulent kinetic energy so that the standard k-ε model overpredicts the axial mean gas velocity along jet centerline.

Figures 4 and 5 displays the radial profiles of the axial mean gas velocity and the turbulent kinetic energy at $x/d_i = 10$, respectively. The radial profiles agree with the observation in the axial evolution. For velocity ratio of 1 and 1.8, the standard k-ε model seems to have a comparable prediction in the turbulent kinetic energy in the outer radial position. This will cause the overprediction of the radial fluctuating gas velocity, which is important parameter in the Lagrangian particle tracking.

For velocity ratio of 0, the flow is a round jet and the standard k-ε model has been known to overpredict the spreading rate because of the overprediction in the gas turbulent kinetic energy. Wilcox noted that a round jet-spreading rate calculated by the standard k-ε model is approximately 18% higher than the experimental data (1). He suggested the drastic surgery of the ε transport equation is responsible for the poor performance of the standard k-ε model. The correct form of the dissipation rate transport equation obtained from the time-averaged Navier-Stokes equation is far more complicated than the k transport equation and involves many unknown double and triple correlations of fluctuating velocity, pressure, and velocity gradient. Many researchers have suggested some modification in the standard k-ε equation to increase the dissipation rate including. adding a cross diffusion term in the k transport equation (2, 3) or modifying C_μ as a function of the ratio of production of gas turbulent kinetic energy to dissipation rate (4).

The poor performance of the standard k-ε model to approximate the flow behavior in a coaxial jet is expected since the presence of the inner shear layer will add more complexity. The inner shear layer can be described similarly as mixing layer or axisymmetric wake. It has been shown that the standard k-ε model tends to underpredict the spreading rate (1, 4). This indicates that the standard k-ε model underpredicts the turbulent mixing in these flows. Since the jet centerline is in the region where the gas

flow behaves as that of mixing layer or wake flow, it is the reason we observed the underprediction in the axial evolution of the gas turbulent kinetic energy. The addition of the cross diffusion term improves the predictability in the mixing layer (3). Modification of C_μ also improves the predictability of the standard k-ε model in the axisymmetric wake (4).

The other important flow variables is the radial mean gas velocity and the radial fluctuating gas velocity, the accuracy of the standard k-ε model is important to predict the radial motion of the particles. Figure 6 shows the radial profiles of the radial mean gas velocity at x/di =3 and 10. The standard k-ε model underpredicts the radial gas mean velocity both in the inner and outer shear layer, causing the overprediction in the calculated drag force. On the other hand, due to the isotropic characteristic of the k-ε model, the standard k-ε seems to overpredict the radial fluctuating gas velocity in the outer shear layer (Not shown). This will overpredict the role of gas turbulence in the radial motion of the particles.

Particle-Phase Flow
Particle Trajectory

Lagrangian particle tracking simulations were performed using the FLUENT 4.5 CFD package. The trajectory of a particle is predicted by integrating the force balance on a particle

$$\frac{\partial u_p}{\partial t} = F_D\left(u_f - u_p\right) + g\frac{(\rho_p - \rho_f)}{\rho_p} + F \qquad (1)$$

Where $F_D\,(u_f\text{-}u_p)$ is the drag force per unit particle mass and

$$F_D = \frac{18\mu}{\rho_p d_p^{\,2}}\frac{C_D\,Re_p}{24} \qquad (2)$$

The drag coefficient, C_D, is a function of the Re_p given by

$$C_D = a_1 + a_2/Re_p + a_3/Re_p^{\,2} \qquad (3)$$

Where a_1, a_2, and a_3 are constants that apply over a range of Re_p (5). Subscript f in this section corresponds to the fluid-phase in the presence of particle. The u_p is the instantaneous velocity of a particle. The second term on the rhs of equation (1) is the gravity force. The third term on the rhs of equation (1) represents the other forces, such as the virtual mass force, F_{vm}, and the force that arises due to the pressure gradient in the fluid, F_p

$$F_{vm} = \frac{1}{2}\left(\frac{\rho_f}{\rho_p}\right)\frac{\partial}{\partial t}\left(u_f - u_p\right) \qquad (4) \text{ and } (5)$$

$$F_p = \left(\frac{\rho_f}{\rho_p}\right) u_p \frac{\partial u_i}{\partial x_i}$$

These two forces are not important for gas-solid flow since the density ratio is small. The other force that is not included in this study is the Saffman Lift force. This force is due to the pressure gradient developed on a particle due to rotation induced by a velocity gradient and can be important in the case with a steep gradient in the gas mean axial velocity.

Two different trajectory methods are considered. The first one is the deterministic-separated flow analysis, DSF, where particle-gas turbulence interactions are ignored. This model represents the fan spreading theory. The second one is the stochastic separated-flow analysis, SSF, where particle-turbulence interactions are considered using a random walk computation for the particles. The continuous Random Walk model, CRW in FLUENT 4.5 was used for the SSF analysis. Particles are assumed to interact with turbulent eddies that have statistically independent properties. Properties inside the eddy are assumed to be uniform, but to change in a random manner from eddy to eddy. Each eddy is characterized by a Gaussian distributed random velocity fluctuation u_f', v_f', and w_f' (angular rms velocity), and by the eddy lifetime, τ_e:

$$\tau_e \approx 2\ T_L$$

$$T_L \approx C_L\ \frac{k_f}{\varepsilon_f} \qquad (6) \text{ and } (7)$$

Where T_L is the integral Lagrangian time constant and C_L is a constant that is set to be 0.15. The effect of crossing trajectory is included in CRW. The crossing trajectory effect arises from the existence of a relative velocity between the gas-phase and particles. The relative velocity will reduce the interaction time between an eddy and particles. CRW in Fluent 4.5 uses the Csanady equation to calculate the reduction of a time interaction (6).

$$\frac{T_L^*}{T_L} = \frac{1}{\left(1 + C\ \left(U_f - U_p\right)^2 \Big/ k_f\right)^{\frac{1}{2}}} \qquad (8)$$

Where T_L^* is the modified fluid Lagrangian integral time, and C is a constant which is set to be 1.5.

Both the DSF and SSF methods need the flow predictions of the gas-phase in the presence of particle. Since the mass loading is low, the modulation of gas-phase by the particles is neglected. Therefore, the single-phase solution was used for the calculation of particle trajectories for all velocity ratios.

Results and Discussion

The trajectory calculations were performed to probe the factors affecting the radial and axial motion of particles. By comparing the calculation using between the DSF method and the SSF, the effect of the gas turbulence on the particle motion can be explored. The initial axial and radial location of particles was 1 mm downstream of the inlet and 2.54 e-4 m from the pipe wall. The initial conditions were matched with the particle-phase data obtained from the LDV measurements.

Figure 7 displays the comparison between the SSF and DSF predictions in the axial particle velocity, u_p for the three velocity ratios. The u is defined as the instantaneous velocity. The results show that the particle axial velocity calculated by the DSF and SSF methods is about the same, verifying that axial particle velocity is controlled mainly by the axial mean gas velocity.

Figure 8 displays the DSF predictions in the radial particle velocity, v_p for the three velocity ratios. The DSF predicts that the drag force plays an important role in reducing the particle radial velocity as is observed in the experiments. The decay rate is about the same for all velocity ratios between the nozzle exit and axial location x/d_i of 2, but they are different between x/d_i of 2 and 10 due to the difference in the velocity ratio. Qualitatively, this Lagrangian predictions agree with the proposed mechanism for the radial mean particle velocity behavior as described previously. The quantitative accuracy of the DSF prediction on the radial particle velocity depends on the accuracy of prediction in the radial mean gas velocity.

The DSF and SSF calculations for the radial particle velocity do not agree with one another. The difference between the DSF and SSF methods in predicting radial particle velocity indicates that the radial fluctuating gas velocity can play a role in the radial motion of particles. The difference in the prediction by the DSF and SSF is surprising since the particle St is larger than 10, but this may be caused by the overprediction of the radial fluctuating gas velocity.

Figure 9 displays the prediction of particle trajectories by both methods for the three velocity ratios. The DSF calculations predict that as the velocity ratio increases, the particle will travel further radially. The SSF prediction shows the same behavior as the DSF prediction by x/d_i of 10. The inaccuracies in the DSF and SSF predictions are caused by the inaccuracy in the standard k-ε turbulence model.

References

1. Wilcox, D.C.," *Turbulence Modeling for CFD*," DCW Industries, California (1998)

2. Jaw S.Y. and Chen, C.J.," Present Status of Second-Order Closure Turbulence Models I: Overview," *J. Eng Mech*, 485-501 (1998)

3. Jaw S.Y. and Chen, C.J.,” Present Status of Second-Order Closure Turbulence Models II: Applications,” *J. Eng Mech*, 502-512 (1998)

4. Rodi, W. ,” *Turbulence Models and Their Application in Hydarulics-A State of The Art Review*,” Balkem, A.A. (1984)

5. Morsi, S.A., and Alexander, A..J.," An Investigation of Particle Trajectories in two-Phase Flow Systems," J Fluid Mech., 55, 193-208, (1972)

6. Csanady, G.T.," Turbulent Diffusion of Heavy Particles in the atmosphere," *J. Atmos. Science*, **20**, 201 (1963).

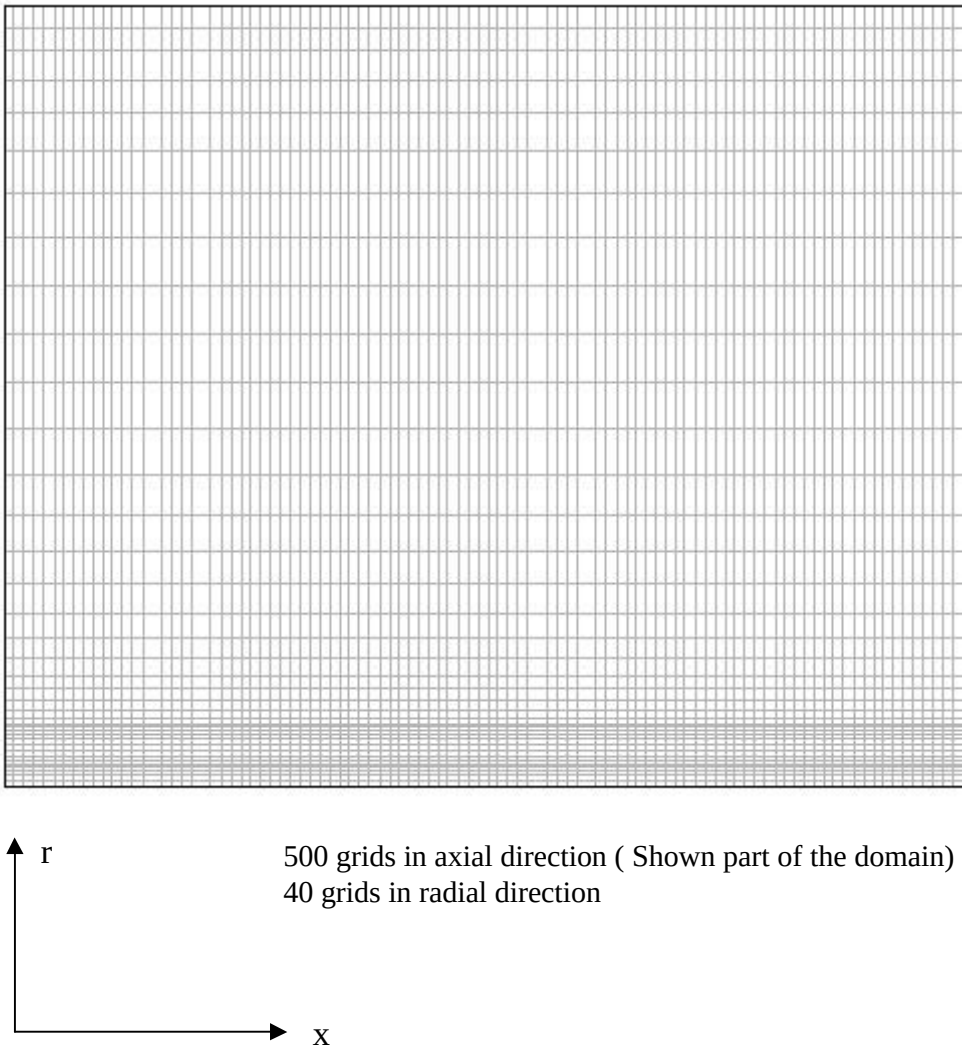

Figure 1. Computational grid used in Fluent 4.5

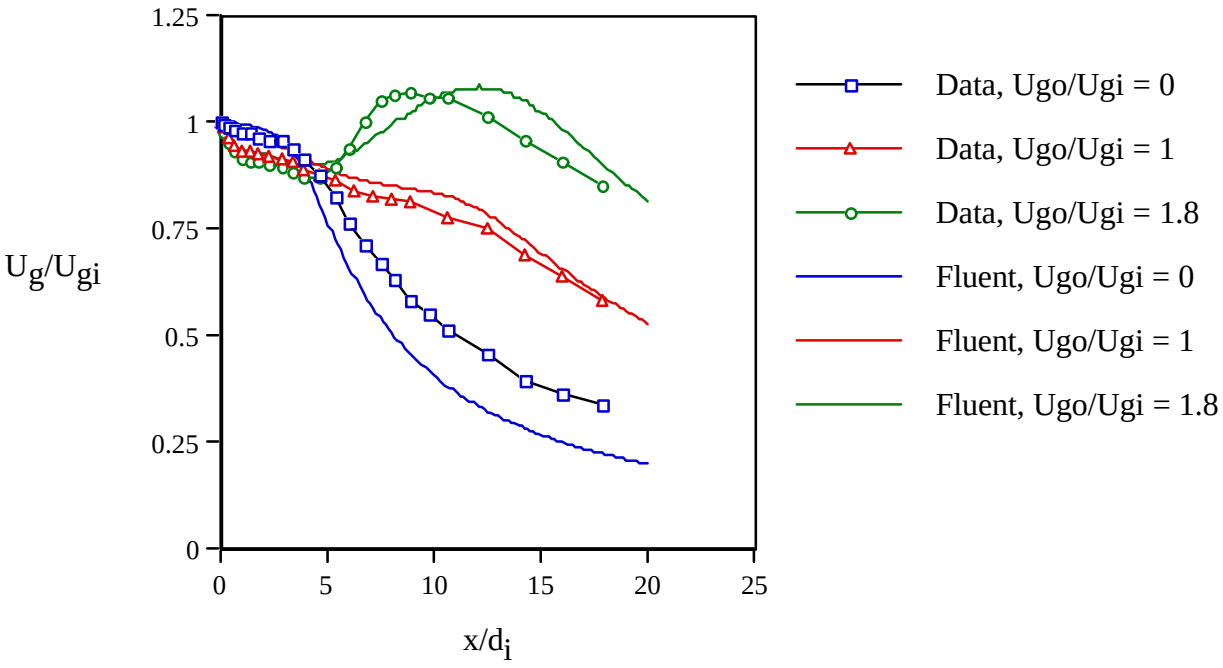

Figure 2. Comparison between the Fluent predictions and experimental data on the axial mean gas velocity along the jet centerline for all Ugo/Ugi

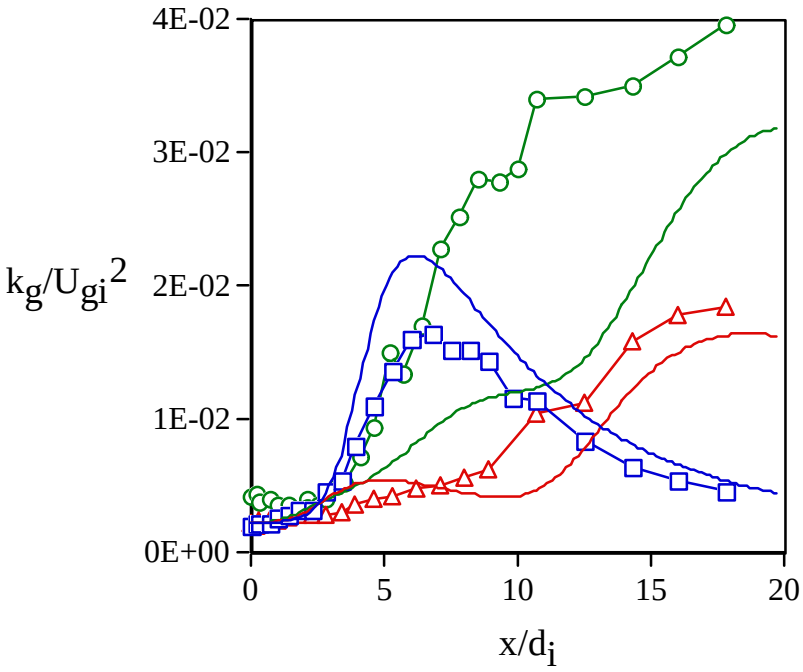

Figure 3. Comparison between the Fluent predictions and experimental data on the turbulence kinetic energy along the jet centerline for all Ugo/Ugi

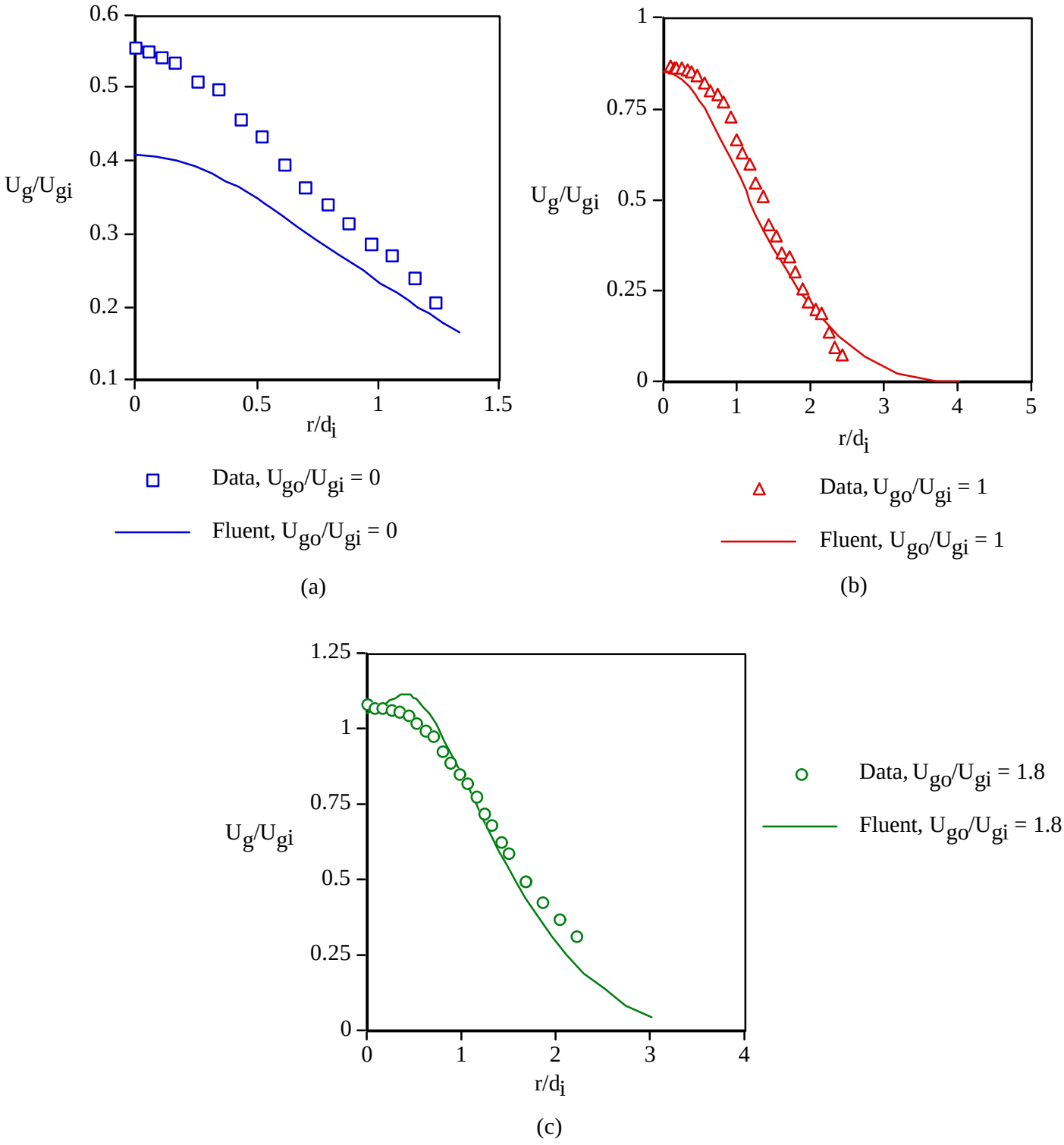

Figure 4. Comparison between the Fluent prediction and experimental data on mean axial gas velocity at x/di = 10 for all velocity ratios

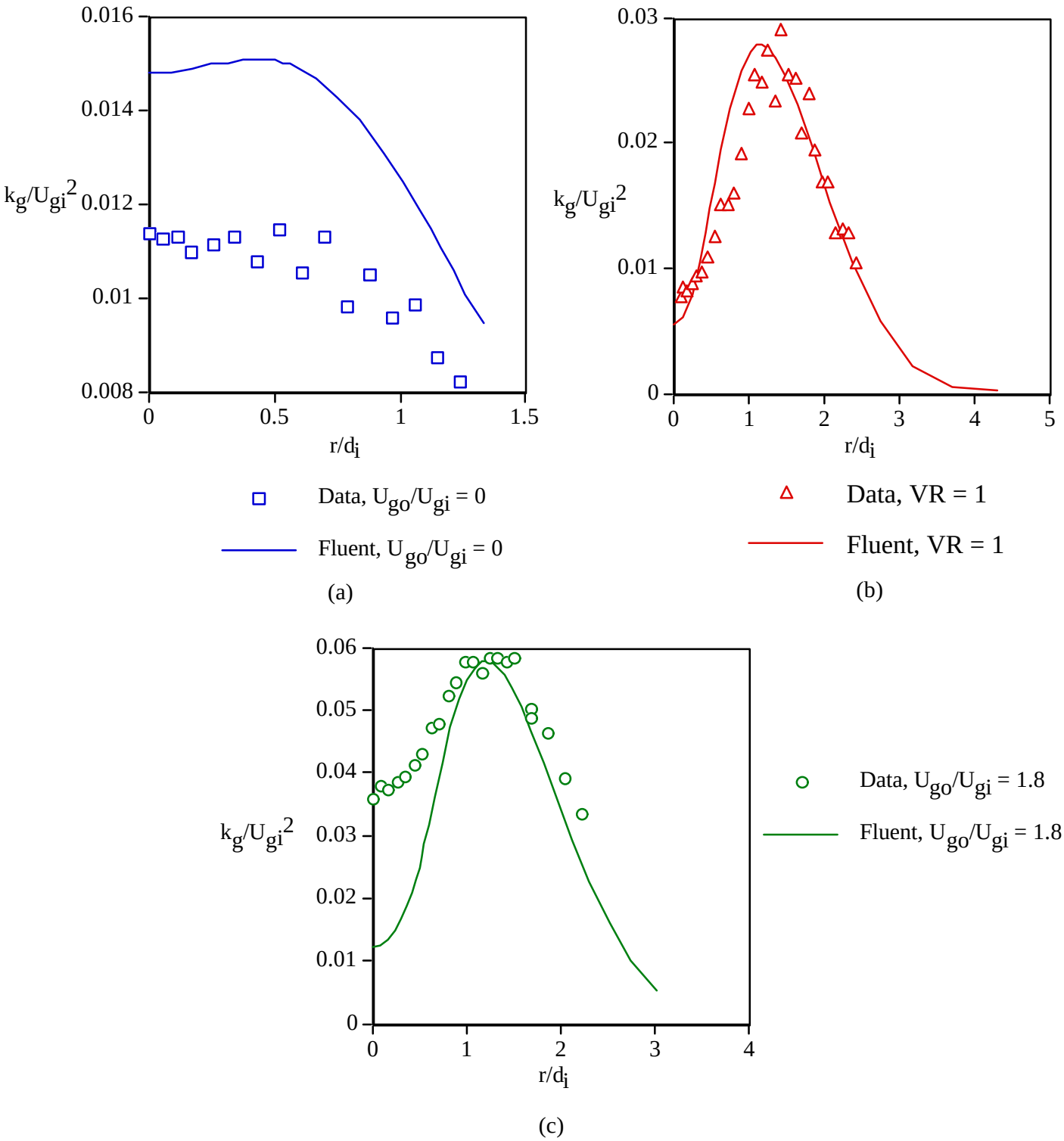

Figure 5. Comparison between the Fluent prediction and experimental data on the gas turbulent kinetic energy at x/di = 10 for all velocity ratios

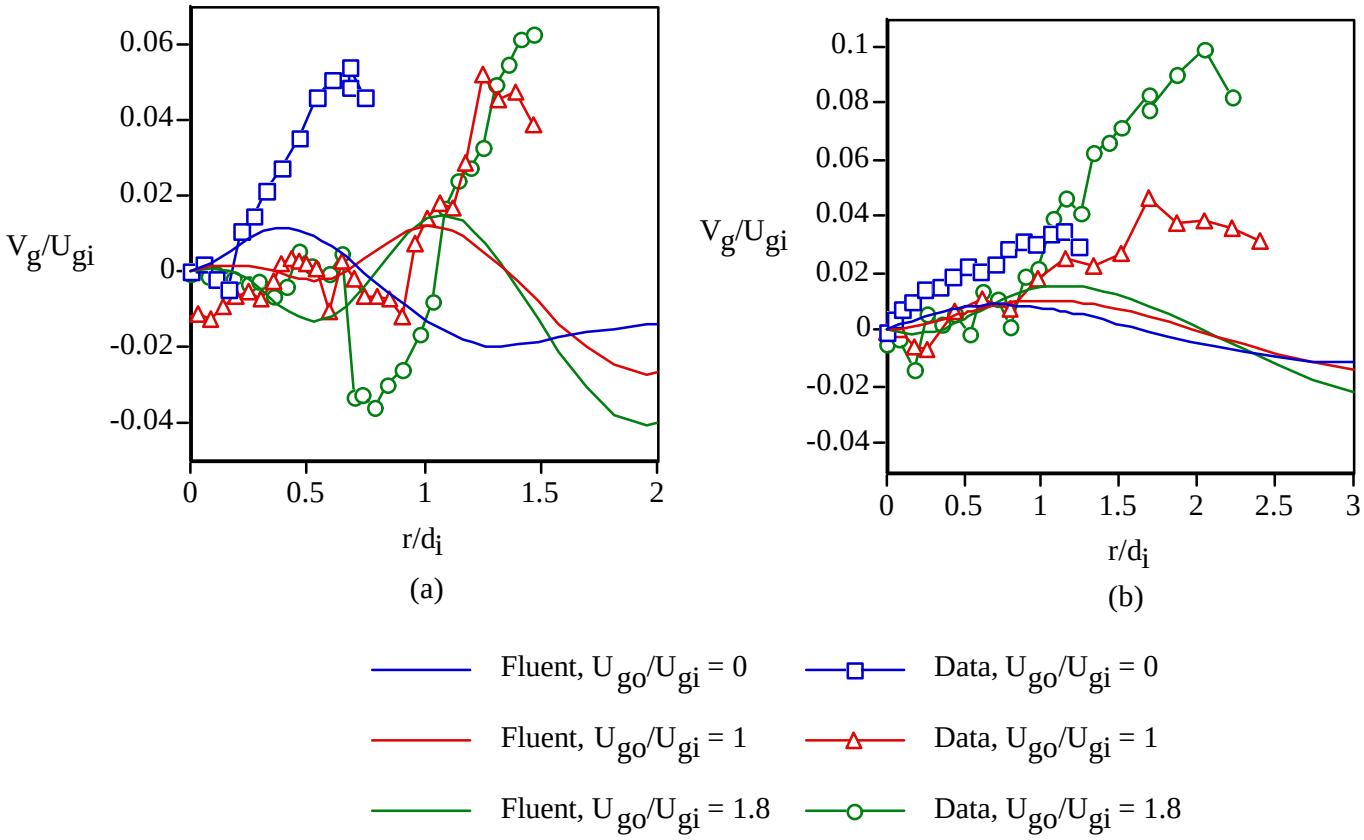

Figure 6. Comparison between Fluent prediction and experimental data on the radial mean gas velocity at (a) x/di = 3 and (b) x/di = 10

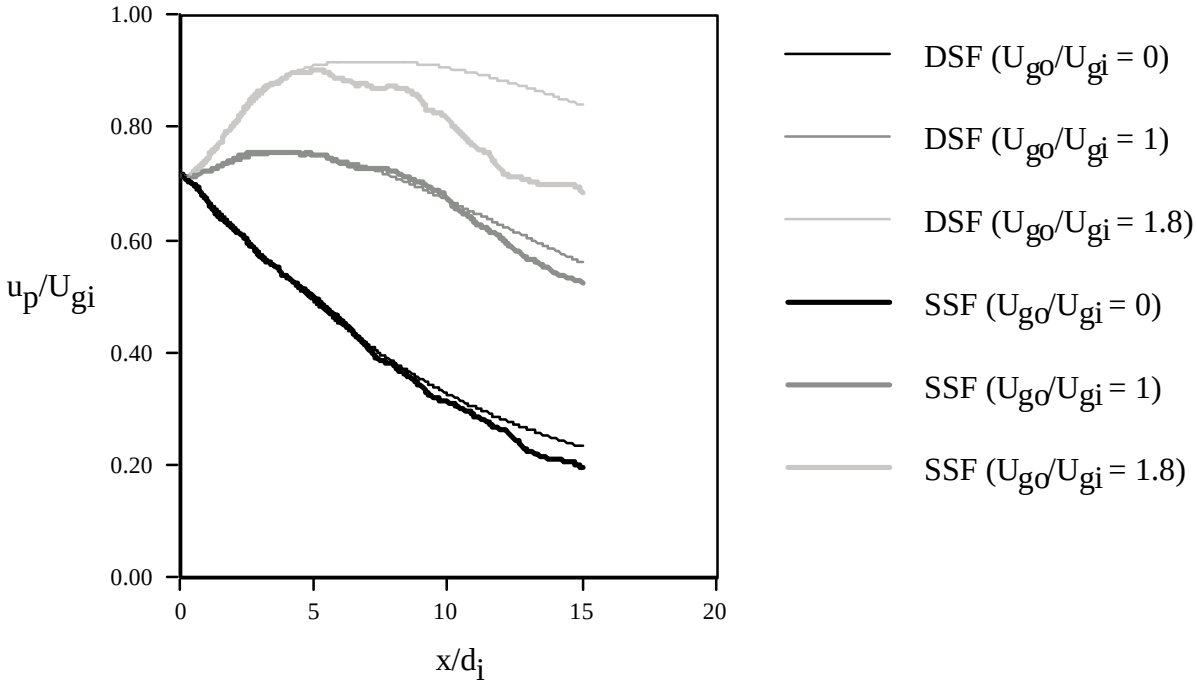

Figure 7. Comparison between the SSF and DSF predictions in the axial particle velocity of the 70 microns glass bead particle for the three Ugo/Ugi

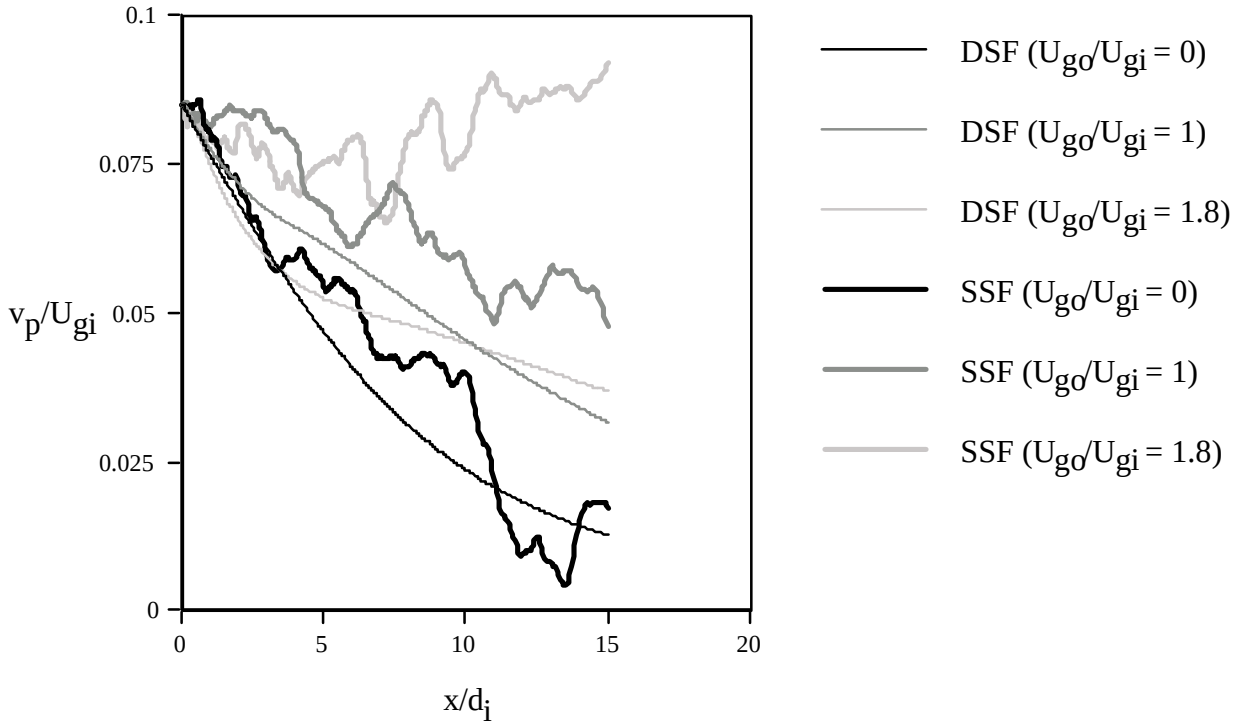

Figure 8. Comparison between the SSF and DSF predictions in the radial particle velocity of the 70 microns glass bead particle for the three Ugo/Ugi

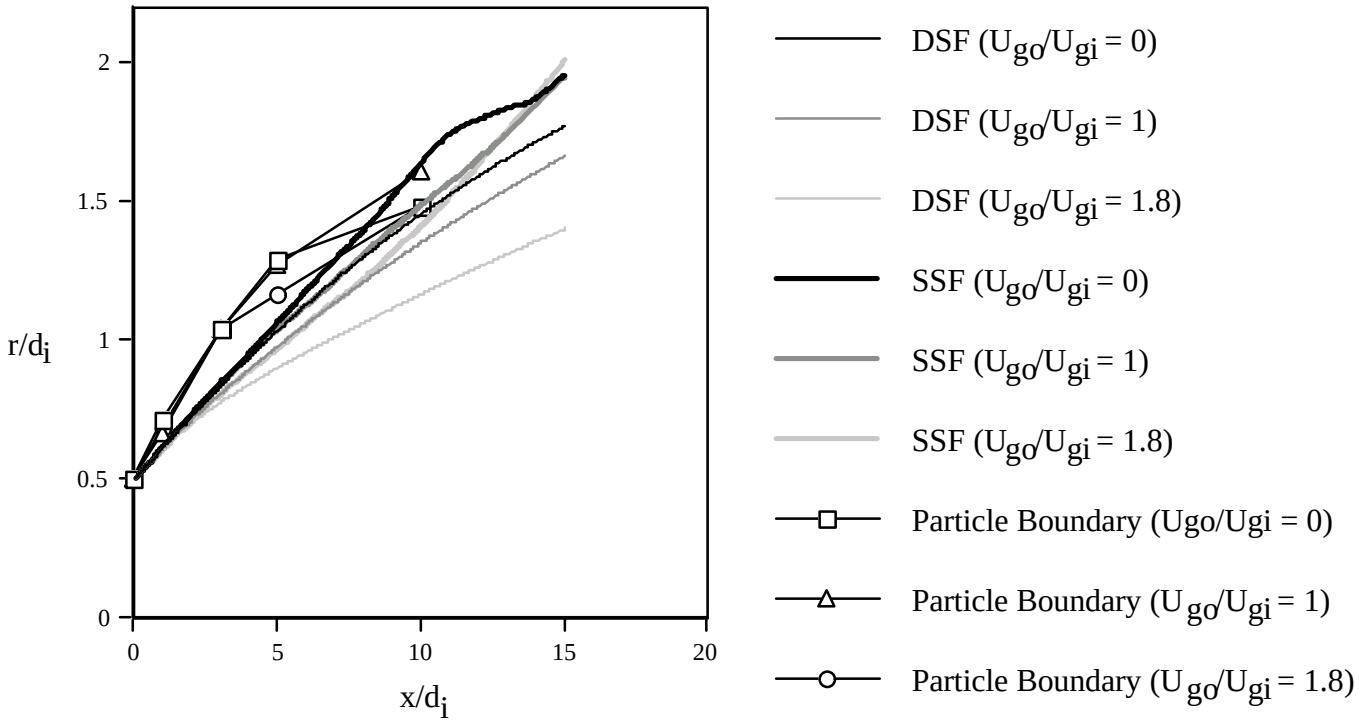

Figure 9. Comparison between the SSF and DSF predictions in the particle trajectories of the 70 microns glass bead particle for the three Ugo/Ugi